https://doi.org/10.5194/cp-2021-94
Preprint. Discussion started: 20 July 2021

Climate of the Past Discussions
Open Access EGU

A theory of glacial cycles: resolving Pleistocene puzzles

Hsien-Wang Ou[1]

[1] Department of Earth and Environmental Sciences, Lamont-Doherty Earth Observatory of Columbia University, Palisades, NY10964, USA (retired)

Correspondence to: Hsien-Wang Ou (hsienou0905@gmail.com)

Abstract. Since the summer surface air temperature that regulates the ice margin is anchored on the sea surface temperature, we posit that the climate system constitutes the intermediary of the orbital forcing of the glacial cycles. As such, the relevant forcing is the annual solar flux absorbed by the ocean, which naturally filters out the precession effect in early Pleistocene but mimics the Milankovitch insolation in late Pleistocene. For a coupled climate system that is inherent turbulent, we show that the ocean may be bistable with a cold state defined by the freezing point subpolar water, which would translate to ice bistates between a polar ice cap and an ice sheet extending to mid-latitudes, enabling large ice-volume signal regardless the forcing amplitude so long as the bistable thresholds are crossed. Such thresholds are set by the global convective flux, which would be lowered during the Pleistocene cooling, whose interplay with the ice-albedo feedback leads to transitions of the ice signal from that dominated by obliquity to the emerging precession cycles to the ice-age cycles paced by eccentricity. Through a single dynamical framework, the theory thus may resolve many long-standing puzzles of the glacial cycles.

1 Introduction

https://doi.org/10.5194/cp-2021-94
Preprint. Discussion started: 20 July 2021

Climate of the Past Discussions

In late Pleistocene, the global ice volume exhibits pronounced variation at orbital frequencies (Hays et al. 1976). As Antarctica is largely iced over since about ten million years ago (Berger 1979), the ice signal reflects mainly that of the northern ice sheet, whose correlation with the Milankovitch insolation supports the latter's control of the ice volume (Milankovitch 1941). The linkage however is necessarily nonlinear since the 100-ky eccentricity contains little power, yet it dominates the ice-age cycles of the late Pleistocene, the so-called "100-ky problem" (Elkibbi and Rial 2001). Equally puzzling, the ice signal exhibits mainly the obliquity periodicity in the early Pleistocene despite the greater precession amplitude (Raymo and Nisancioglu 2003), and then the mid-Pleistocene transition (MPT, all acronyms are listed in Appendix A) from the obliquity- to the eccentricity-dominated ice cycles is not accompanied by appreciable change in the Milankovitch insolation (Clark et al. 2006). Given the distinctness of these features, they should emerge from fundamental physics of the climate-cryosphere system, which is yet to be delineated.

The above observations have weeded out some previous resolutions of the 100-ky problem, as briefly recounted below. Early attempts have invoked internal oscillations of the ice sheet due to mass-balance feedback or isostatic adjustment (Weertman 1976; Imbrie and Imbrie 1980; Oerlemans 1982; Pollard 1983; Pelletier 2003), but these are broadband processes, which would elevate the low-frequency variance but not produce a spectral peak coincidental with the eccentricity (Imbrie et al. 1993). Others have invoked stochastic or chaotic dynamics in conjunction with the orbital forcing (Wunsch 2003; Huybers 2009), which however may be at odds with the observation that ice ages seem to always terminate at rising eccentricity

https://doi.org/10.5194/cp-2021-94
Preprint. Discussion started: 20 July 2021

(Raymo 1997; Kawamura et al. 2007; Lisiecki 2010), suggesting a more deterministic process (Meyers and Hinnov 2010). Both internal oscillations and stochastic dynamics may not explain why they are not operative in early Pleistocene when the northern hemisphere glaciation has already set in (Ravelo et al. 2004) and yet 100-ky cycles are absent. Then there are conceptual or dynamical-system models (Saltzman et al. 1984; Ghil 1994; Paillard 1998; Tziperman et al. 2006; Imbrie et al. 2011; Crucifix 2013; Daruka and Ditlevsen 2016), which can be tuned to replicate the observed signals, but since key parameters are not linked to measurable quantities, these models are mostly unfalsifiable as more parameters invariably lead to better fit, which also has limited prognostic utility since free parameters may not be assumed fixed for a changed forcing scenario.

A more palpable paradigm is that the ice sheet is bistable (Weertman 1976), so the hysteresis can be triggered by eccentricity-modulated forcing to produce the 100-ky cycle, and if the hysteresis thresholds is lowered by the putative decrease of the atmospheric CO_2 during the Pleistocene, one has a possible explanation of the MPT (Berger et al. 1999; Calov and Ganopolski 2005; Abe-Ouchi et al. 2013). But there is no evidence of such CO_2 trend (Honisch et al. 2009), which moreover is likely a response than a cause of the climate change (Petit et al. 1999; Siegenthaler et al. 2005; Honisch et al. 2009), and then the atmospheric CO_2 in any event has only minor effect on the temperature (Broecker and Denton 1989; Petit et al. 1999), the reason that the model-produced temperature range is small compared with the observed one (Abe-Ouchi et al. 2013). One serious difficulty of the above hysteresis is that one of the bistates is an ice-free state, so the ice signal is minimal prior to the MPT (Berger and Loutre

https://doi.org/10.5194/cp-2021-94
Preprint. Discussion started: 20 July 2021

2010, Fig. 2), which is at odds with the substantial obliquity signal observed in early Pleistocene (Letreguilly et al. 1991; Raymo and Nisancioglu 2003; Lisiecki and Raymo 2007). We shall argue later (Sect. 3.3) that an ice-free state is untenable in the Pleistocene, so the hysteresis paradigm, if it were to apply, must involve different bistates, which as we shall see can be engendered by the ocean.

Not sufficiently acknowledged in above studies is the central role played by the ocean. Physically, the summer surface air temperature (SAT) that controls the ice margin is anchored by the sea surface temperature (SST), so the ocean must constitute the primary entry of the radiative forcing into the climate-cryosphere system (Broecker and Denton 1989). Observationally, the meridional overturning circulation (MOC), the SST and the SAT all covary strongly during glacial cycles (Ruddiman et al. 1986; Imbrie et al. 1992, Fig. 6; Keigwin et al. 1994, Fig. 2; Lisiecki et al. 2008; Nie et al. 2008), which arguably precede the ice-volume signal by several millennia, suggesting a causal linkage (Petit et al. 1999; Shackleton 2000; Medina-Elizalde and Lea 2005). In addition, it is noted that abrupt climate changes involve MOC jumping between modes (Broecker et al. 1985; Alley et al. 2000), a bistability that has been demonstrated by coupled climate models (Manabe and Stouffer 1988) whose dynamical basis however remains unclear. To remedy this shortfall, this author (Ou 2018) has recently extended Stommel's (1961) ocean-only model to include the atmospheric coupling, which reveals bistates that depend on the forcing timescale. For sub-millennial timescale, they are the ones

https://doi.org/10.5194/cp-2021-94
Preprint. Discussion started: 20 July 2021

seen in coarse-grain numerical models, but for orbital timescales, the bistates are set by an entropy principle of the nonequilibrium thermodynamics (NT) and hysteresis can be triggered by the modulated orbital forcing.

Justified on both physical and observational grounds, we posit therefore that the coupled climate system constitutes the intermediary of the orbital forcing of the glacial cycles. Diametrically opposite to numerical models that often add poorly constrained physical elements to improve the simulations, our approach seeks to isolate minimal physics that may account for the observed phenomenon. As organized below, our theory consists of two parts: the elucidation of the inner working of a coupled climate system, and the filtering of the orbital forcing through this system to generate glacial cycles; the two parts are contained in Sect. 2 and 3, respectively. In Sect. 4, we summarize the essence of the theory and discuss how it may resolve many Pleistocene puzzles of the glacial cycles.

2 Coupled climate model

In striving for minimal physics, we consider a model configuration of the North Atlantic as sketched in Fig. 1, for which both ocean and atmosphere are divided into warm and cold masses by mid-latitude fronts and an ice sheet may form on the adjacent continental strip terminating at the Arctic Ocean (all symbols are defined in Appendix B). The ocean is heated by the annual absorbed shortwave (SW) flux, which heats the overlying air by the convective and

https://doi.org/10.5194/cp-2021-94
Preprint. Discussion started: 20 July 2021

net longwave (LW) fluxes, the latter assumed spatially uniform. Since glacial cycles are dominated by the subpolar temperature, the model variables pertain to the cold-box deviations from the global-means, the latter assumed known.

2.1 Regime diagram

The derivation of the model is provided in Ou (2018) to which the readers are referred for details. Sufficing for the present purpose, we shall summarize the model solution and its underlying physics via a regime diagram shown in Fig. 2 whereby the cold-box deviations from the global-means are plotted against the MOC (*K*). All variables have been nondimensionalized (hence primed) whose scaling definitions and their standard values are listed in Appendix B. This regime diagram is drawn for a forcing of $q' = 1$ and a global convective flux of $\bar{q}_c' = .75$.

For an infinite K, the ocean is homogeneous, so the cold-box SST deficit (T') is zero and the cold-box SAT (T_a') is colder by the global convective flux ($\bar{q}_c'$). As K decreases, the subpolar water cools, which cools the overlying air and induces an atmospheric heat transport, the latter in turn weakens the ocean heat transport (the total heat transport is fixed by q') hence reduces the steepness of the temperature curves. There is however an upper limit to the atmospheric heat transport since the convective flux (the spacing between two temperature curves) cannot be negative, which occurs at

$$T' = 2\bar{q}_c'. \qquad (1)$$

https://doi.org/10.5194/cp-2021-94
Preprint. Discussion started: 20 July 2021

Climate of the Past Discussions

Beyond this "convective bound", the atmospheric heat transport has saturated, and the two temperature curves would merge to steepen at the same faster rate (inverse in *K*).

Since the moisture transport is proportional to the atmospheric heat transport on account of the Clausius-Clapeyron Equation (Ou 2007), the increasing atmospheric heat transport with decreasing *K* implies a salinity deficit (S') that increases faster than temperature deficit T' before the convective bound, but at the same rate afterward when the atmospheric heat transport has saturated. The disparate slopes of the two curves result in a density surplus ($\rho' = T' - S'$) that has opposite slopes straddling the convective bound, the latter thus divides the climate regime into warn and cold branches, a robust outcome of the atmospheric coupling.

To specify the climate state from the continuum of these curves, one needs a constraint on the MOC, which is customarily assumed linear in the density surplus (Stommel 1961; Marotzke and Stone 1995) as indicated in the thick dashed line. The proportional constant (the inverse of the slope) is referred as the admittance and the line, the admittance line whose intersects with the density curve then specify the climate state. For the admittance chosen, the ocean has two stable states (solid ovals) enclosing an unstable saddle point (open oval), a bistability that is predicated on the convective bound hence the ocean/atmosphere coupling.

The presence of the cold state has been demonstrated by coupled numerical models (Manabe and Stouffer 1988), which indeed is characterized by vanishing convective flux over the subpolar water (their Fig. 17), as predicted by the convective bound. As its further computational support, coupled models have shown hysteresis when the freshwater flux is perturbed

https://doi.org/10.5194/cp-2021-94
Preprint. Discussion started: 20 July 2021

(Rahmstorf et al. 2005), which can be readily gleaned from the regime diagram. In these numerical models, which do not resolve eddies, the admittance depends sensitively on the diapycnal diffusivity --- a highly uncertain property of the ocean, which is in effect finely tuned to replicate the observed state (Rahmstorf et al. 2005). Moreover, the hysteresis caused by changing radiative flux would be of the opposite sign of --- hence plays no part in --- the glacial cycles: a stronger radiative flux, for example, would raise the temperature curve (hence lower the density curve) to cause transition to the cold glacial instead of the warm interglacial. The culprit lies in the fixed admittance line of a *laminar* ocean, which can be justified only for short-term sub-millennial climate changes (Ou 2018), but must be relaxed for the orbital forcing of a *turbulent* ocean, as discussed next.

2.2 Ocean bistates

Differing from the laminar ocean of coarse-grain numerical models, the actual MOC is subjected to microscopic fluctuations associated with random eddy exchanges across the subtropical front. Applying the fluctuation theorem (Crooks 1999), Ou (2018) deduces that the admittance is not fixed but would evolve on millennial "entropy adjustment" time toward the maximum entropy production (MEP). The latter thus is a veritable generalization of the second fundamental law to nonequilibrium thermodynamics (NT, Ozawa et al. 2003), which has been applied previously to climate theories (Kleidon 2009). We blur the admittance line by a shaded cone to signify fluctuations, which thus would slowly pivot by increasing entropy production until it attains maximum marked by solid ovals.

https://doi.org/10.5194/cp-2021-94
Preprint. Discussion started: 20 July 2021

As derived in Ou (2018), the warm MEP state is given by

$$(T', K) = (q', 1/2), \tag{2}$$

which defines our interglacial. As a crude check, applying standard parameters (Appendix B) yields a subpolar SST of 6 ^{0}C and MOC of 14 Sv (for a basin width of $6 \times 10^3 km$), not unlike the present interglacial (Peixoto and Oort 1992; Macdonald 1998). It should be noted that since our MOC does not depend on the uncertain diapycnal diffusivity, it is more robust than that produced from coarse-grain numerical models.

The cold MEP on the other hand is characterized by low-salinity subpolar water at the freezing point T_f', which is consistent with the observed one during last glacial maximum (LGM, CLIMAP 1976; Duplessy et al. 1992) hence referred as the glacial state. It is significant that although the subpolar water is at the freezing point, it remains ice-free; this is because the sea ice would curb the ocean heat loss to weaken the MOC hence the entropy production, in contradiction to the MEP. This deduction however applies only for timescales long compared with the millennial entropy adjustment time, so it does not preclude the extensive sea-ice formed at the onset of the Heinrich events or during the termination of ice ages (Broecker 1994; Denton et al. 2010). Incidentally, since the sea ice has little thermal inertia hence can be present *only* when the water is at the freezing point, it can play no active role in regulating the glacial cycles, as previously conjectured (Gildor and Tziperman 2003).

2.3 Hysteresis

https://doi.org/10.5194/cp-2021-94
Preprint. Discussion started: 20 July 2021

Climate of the Past
Discussions
Open Access
EGU

With the bistable MEP shown in Fig. 2, one readily discerns possible hysteresis when the orbital forcing varies, as illustrated in Fig. 3. Suppose one is at the warm state (solid circles), a reduction in the absorbed solar flux would cool the temperature, as indicated by the solid arrows and open circles. When the temperature cools to below the convective bound (the horizontal dashed line marked $2\bar{q}_c'$), the warm MEP no longer exists, and the ocean would enter the cold branch to propel toward the cold MEP. With (1) and (2), this cold transition q_c' occurs at

$$q_c' \equiv 2\bar{q}_c', \tag{3}$$

a function only of the global convective flux, an external parameter. Now suppose one is at the cold MEP of freezing point (solid squares), then a rising absorbed solar flux would raise the temperature curve to propel the cold state, as indicated by dashed arrows and open squares. The flattening of the admittance line combined with random fluctuations would vault the climate state into the warm branch, followed by its propelling toward the warm MEP. As a conservative upper bound on the warm transition q_w' , one may set a level admittance line to yield (Ou 2018, from his Eqs. 8 and 12)

$$q_w' \equiv (1+\mu)\bar{q}_c' , \tag{4}$$

where μ is related to the moisture content of the atmosphere with a standard value of about .3. The above two thresholds define the bistable interval, which thus is a function only of the global convective flux. As the latter is decreasing during the Pleistocene cooling, its interplay

https://doi.org/10.5194/cp-2021-94
Preprint. Discussion started: 20 July 2021

Climate of the Past Discussions

with the ice-albedo feedback and forcing modulation is seen later to produce varied glacial cycles.

3 Glacial cycles

To translate the possibility of climate hysteresis to particulars of glacial cycles, we need to first determine the relevant orbital forcing, as discussed next.

3.1 Orbital forcing

Because the thermal inertia of the ocean has integrated the seasonal cycles, the relevant orbital forcing is the annual absorbed SW flux integrated over the subpolar water. Being the annual mean, the forcing is dominated by that over high latitudes, which is about an order greater than that over the tropics (Berger et al. 2007, Fig. 2.7); and then over high latitudes, the forcing is dominated by the summer insolation due both to the vanishing hence unvarying winter insolation (Berger 1988, Fig. 18b; Tricot and Berger 1988, Fig. 4b) and to the ice-albedo feedback that amplifies the summer forcing. Here we must stress the necessity of the ice-albedo feedback in instituting the precession forcing without which its annual absorbed flux is zero because of the Kepler's law. To avert this stricture, Huybers (2006) has posited a higher but unspecified melt threshold in late Pleistocene, but with the forcing being the absorbed flux, the ice-albedo feedback provides a palpable and quantifiable effect, as estimated next.

In early Pleistocene before the activation of the ice-albedo feedback, the forcing would be limited to the obliquity on account of the Kepler's law. In late Pleistocene when the ice

https://doi.org/10.5194/cp-2021-94
Preprint. Discussion started: 20 July 2021

sheet may grow to mid-latitudes, the ice-albedo range can be as large as 0.3 (CLIMAP 1976, Fig. 1), which would incur a range in the absorbed flux of 150 $W \cdot m^{-2}$ given the summer insolation of 500 $W \cdot m^{-2}$. Adding the obliquity range of 40 $W \cdot m^{-2}$ (Imbrie et al. 1993, Fig. 1), the total range is 190 $W \cdot m^{-2}$, which would be halved to 95 $W \cdot m^{-2}$ for the annual mean. Noting that integration over the subpolar water has allayed the latitudinal difference of the obliquity and precession forcing, and reduced by half the excess atmospheric attenuation over the global mean to about 10% (Tricot and Berger 1988, Fig. 1), hence both are neglected.

With the above estimates, we see that the late Pleistocene forcing is comparable to the Milankovitch insolation (Imbrie et al. 1993, Fig. 1), which thus may be taken as its proxy. We should stress that our use of the Milankovitch insolation is not because of its direct effect on the summer SAT or ablation, as widely applied, but because it mimics the annual absorbed flux that drives the SST, on which the summer SAT anchors.

3.2 Summer SAT

Since ice ablation is controlled by the summer SAT (Pollard 1980), the latter needs to be linked to the annual SAT determined from our climate model (Fig. 2). The increasing continentality with latitudes induces strong latitudinal variation of both the annual and the seasonal SAT (Oerlemans 1980; Donohoe and Battisti 2013), which on the other hand is smoothed by the atmospheric motion. Because of these complications, it would seem intractable to deduce the summer SAT from the heat balance, and indeed its calculation by numerical models typically involves adjusting the eddy diffusivity to replicate the observed SAT (Oerlemans 1980;

https://doi.org/10.5194/cp-2021-94
Preprint. Discussion started: 20 July 2021

North et al. 1983). To circumvent such empirical tuning that necessarily degrades its prognosis, we discern nonetheless a robust constraint on the summer SAT from observations (Peixoto and Oort 1992, Fig. 7.5), namely, it is near the freezing point at the edge of the Arctic Ocean, which can be reasoned below on physical grounds.

We first argue that the summer air cannot be consistently warmer than the freezing point since it would melt the perennial ice to contradict its emergence since about 3 million year ago (Clark 1982; Ravelo et al. 2004). We then argue that the summer air may not be consistently colder than the freezing point either since the Arctic Ocean would then freeze over, which contradicts an ice-free North Atlantic on account of the MEP (Sect. 2.2) and its entry into the Arctic Ocean that would maintain open coastal water.

At the southern end of the subpolar water, because of the much reduced continentality hence seasonal cycle, the summer SAT can be approximated by the annual SAT determined from our climate model. Having pinned down the two end points, we then invoke the atmospheric dynamics to connect them with a straight line, as seen in Fig. 4 (the thick solid line for the interglacial). The summer SAT would pivot about the freezing point at its northern end by the orbital forcing (the shaded cone) whereas for the glacial state, it would assume a uniform freezing point throughout the subpolar region hence overlay with the abscissa, a deduction that is consistent with LGM simulations (Clark et al. 1999, Fig. 2).

3.3 Ice margin

https://doi.org/10.5194/cp-2021-94
Preprint. Discussion started: 20 July 2021

Assuming a constant lapse rate, the summer SAT profile shown in Fig. 4 also represents the snowline whose intersect with the southern face of the ice sheet defines the equilibrium line (EL). To determine the equilibrium line altitude (ELA) h_0 hence the ice margin, we need to consider both the ice dynamics and the mass balance and, given the myriad processes involved, we shall retain only the minimal physics. For the ice dynamics, we assume a perfect plasticity with yield stress τ_i, so the momentum balance yields (see Van der Veen 2013)

$$d(h^2) = -c \cdot dx \tag{5}$$

where h is the height of the southern face of the ice sheet and $c \equiv (g\rho_i)^{-1}(2\tau_i)$ with g, the gravitational acceleration and ρ_i, the ice density. We assume an ablation rate given by νT_i where T_i is the ice surface temperature (above the freezing point) and ν, an empirical constant (Pollard 1980), and let l_0 and l be the x-coordinates of the EL and ice margin, respectively, then the annual ablation is, invoking (5),

$$A_b = \int_{l_0}^{l} \nu T_i dx$$

$$\approx \frac{\nu\gamma}{c} \int_{h_0}^{0} (h_0 - h)\, d(h^2)$$

$$= \frac{\nu\gamma}{3c} h_0^3, \tag{6}$$

which thus depends strongly on the ELA. The accumulation A_c is simply the moisture flux crossing the EL, which can be linked to the energy flux and the local moisture content --- both

https://doi.org/10.5194/cp-2021-94
Preprint. Discussion started: 20 July 2021

are strongly constrained by the EL being at the freezing point (Ou 2007). For this reason, the accumulation would be largely insulated from the varying surface climate associated with the glacial cycles and even further removed from the changing latitudinal gradient of the summer insolation (Raymo and Nisancioglu 2003). Equating the ablation and accumulation, we derive the ELA

$$h_0 \approx (\frac{3cA_c}{\nu\gamma})^{1/3}, \quad (7)$$

which is estimated next.

Given the above constraint on the moisture flux by the freezing-point EL, we shall approximate it by the summer moisture flux into the Arctic Ocean as the latter is rimmed by the freezing temperature. Based on Peixoto and Oort (1992, Fig. 12.21), this moisture flux is estimated to be $A_c = 2 \times 10^5 m^2/y$. Setting additionally τ_i =1 bar (Van der Veen 2013) so that $c = 22\ m$, $\nu = 2\ m$ (y ^{0}C)$^{-1}$ (Pollard 1980) and $\gamma = 6\ ^0C\ km^{-1}$, we estimate $h_0 = 1\ km$, which is like that observed over the current Greenland ice sheet (Oerlemans 1991). This ELA implies an ice margin aligned with the summer isotherm of 6 ^{0}C, which may explain why the Greenland is largely ice-covered as this isotherm is located near its southern edge (North et al. 1983, their Fig. 5b). North et al. (1983) has pegged the ice margin at the summer 0 ^{0}C isotherm, which is deficient since there would be no summer ablation to counter the yearly accumulation, and then it would imply an ice-free Greenland, contradicting the observed one. Although the parameters in (7) are uncertain, the sensitivity is somewhat dampened by the 1/3

https://doi.org/10.5194/cp-2021-94
Preprint. Discussion started: 20 July 2021

power, so our pegging of the ice margin with the summer isotherm of O (10 ^{0}C) should generally apply.

With the above estimates, the interglacial ice sheet (the medium shade in Fig. 4) extends about 1/3 toward the subtropical front and the ice margin would vary linearly with the forcing (the dark cone), which we shall categorize as the polar ice cap, such as the present Greenland ice sheet. For the glacial state, the summer SAT is at the freezing point throughout the subpolar region, so the ice sheet would extend to the subtropical front (lightly shaded) corresponding to the Laurentide ice sheet (LIS). It is seen therefore that the ocean bistates would translate to ice sheet of vastly different sizes, resulting in a large ice-volume signal regardless the forcing range so long as the bistable thresholds are crossed.

The large ice signal thus differs fundamentally from that associated with the inherent ice bistates of polar ice cap and ice-free state. And then with the surface snowline hovering around the edge of the Arctic Ocean (Sect. 3.2), it is readily seen from Fig. 4 that the ice-free state is unstable: a slight southward migration of the snowline would produce a finite polar ice cap via the mass-balance feedback, yet its erasure requires a warming of about 6 ^{0}C accompanied by a northward snowline migration of O (1000 km) (the dashed line), an unlikely perturbation. This deduction of a stable polar ice cap is consistent with numerical studies, which show that the current Greenland ice sheet would melt away only with more than 5 ^{0}C warming (Letreguilly et al. 1991).

3.4 Mid-Pleistocene transition (MPT)

https://doi.org/10.5194/cp-2021-94
Preprint. Discussion started: 20 July 2021

The MPT from the obliquity- to the eccentricity-dominated ice-volume cycles has posed a significant challenge to the astronomical theory since the Milankovitch insolation displays no discernible change. Besides the decreasing CO_2 trend that we have critiqued in Sect. 1, the changing substrate geology has also been postulated (Clark et al. 2006); both however represent extraneous physics to the Pleistocene cooling, which is likely tectonic in origin (Ruddiman and Raymo 1988). Instead, as a direct consequence of the Pleistocene cooling, we argue that the global convective flux would be lowered. This is because the cooling implies a drier air hence a smaller downward LW flux (Ou 2001, Fig. 2), which then requires a smaller global convective flux for the ocean heat balance --- all else being equal. Significantly, the global convective flux is precisely what sets the bistable interval of our climate, and we shall see its interplay with the ice-albedo feedback provides a natural account of the MPT. There are of course no proxy data for the convective flux, so its reduction during the Pleistocene cooling can only be supported by the seeming robust physics and its potency in explaining the MPT.

Based on the discussion to follow, we show the Pleistocene evolution of the forcing and ice signals in Fig. 5 (time proceeds to the left), which consists of three stages and their transitions. The three stages correspond roughly to the three periods depicted in Imbrie et al. (1993, their Fig. 3) and the two transitions, the early and middle Pleistocene transitions identified by Lisiecki and Raymo (2007). For illustrative purpose, the forcing is represented by a shaded envelop (neglecting the obliquity and precession periods) centered on the thick dashed line (referred as the mean forcing) and the forcing markers along the right ordinate are merely indicative. The vertical bars are bistable intervals spanned by the cold and warm thresholds given in

(3) and (4), which are slowly approaching the horizontal axis as the global convective flux decreases during the Pleistocene cooling.

At Stage 1 in the warm early Pleistocene, there is little ice-albedo feedback to effectuate the precession forcing (Sect. 3.1), so the ice signal is simply that of the polar ice cap linearly perturbed by the obliquity forcing. This Stage 1 can be identified with the time span before 1.5 Ma (million years ago), which thus is dominated by interglacial cycles at the 41-ky obliquity period. The continuing cooling would enhance the ice-albedo feedback hence the precession forcing, both attaining maxima when the deepest precession trough q'_{max} exceeds the cold threshold (3) to generate the glacial state. This being the precondition of the full-fledged precession forcing that defines Stage 2, we thus set (from Eq. (3))

$$\bar{q}'_c = q'_{max}/2 \qquad (8)$$

as a crude marker for the early Pleistocene transition (EPT) from Stage 1 to 2. As the glacial state is not yet generated prior to Stage 2, the ice signal varies linearly with the forcing, so the EPT can be identified with the time span of 1.5-1 Ma based on the observed ice signal (Imbrie et al. 1993, Fig. 3). Since the ice-albedo feedback primarily depresses the precession troughs but not its peaks, the precession broadening of the forcing envelop should manifest in the deepening of its mean, as indicated in the figure. This should reflect in the SST and ice volume, which indeed is a pronounced feature in observations (Imbrie 1993, Fig. 3; McClymont et al. 2013, Fig. 8).

https://doi.org/10.5194/cp-2021-94
Preprint. Discussion started: 20 July 2021

Stage 2 is defined by full-fledged precession forcing (hence modulated by eccentricity) when the bistable centerline still lies below the mean forcing. Although glacial states are now generated by deep precession troughs during high eccentricity, they are invariably nullified by the next precession peaks, and the phase span of this bistate oscillation is lighter shaded to symbolize the presence of substantial ice sheet. Outside this phase span, the precession troughs no longer clear the cold threshold so there is only interglacial ice signal (dark-shaded) varying linearly with the precession forcing. We shall identify Stage 2 with the time span of 1 to .7 Ma, which thus is characterized by the emerging glacial/interglacial (G/IG) cycles at the 21-ky precession period.

The continuing cooling causes the bistable centerline to rise above the mean forcing, which defines Stage 3. There are again bistate oscillations during high eccentricity indicated by the lighter shade, outside of which however the precession peaks no longer clear the warm transition, so the glacial state would persist through the low eccentricity to allow the full growth of the ice sheet to mid-latitudes. This prolonged glacial state of extensive ice sheet defines the ice age, which is symbolized by the unshaded forcing envelop. Stage 3 thus is dominated by ice-age cycles at the 100-ky eccentricity period, which corresponds to the observed time span of .5 Ma to the present. It is seen from the figure that since the ice age terminates and commences at the same warm threshold, there is no need to invoke differing physics for their occurrences, as suspected previously (Broecker et al. 1985; Raymo 1997).

The MPT from Stage 2 to 3 thus spans the time interval of .7-.5 Ma when the bistable centerline crosses the mean forcing, which can be seen from (3)-(4) to be given by

https://doi.org/10.5194/cp-2021-94
Preprint. Discussion started: 20 July 2021

Climate of the Past Discussions

$$\bar{q}_c' = \frac{2}{3+\mu}\bar{q}^t. \tag{9}$$

While the precession is not of zero period, nor are the transitions sharply defined, which may spread over several hundred thousand years, so the above criteria may provide crude markers of the two transitions. For a cursory check of these criteria, we set a mean forcing of 100 $W \cdot m^{-2}$ and a forcing amplitude of 50 $W \cdot m^{-2}$, then EPT and MPT would be marked by global convective fluxes of 75 $W \cdot m^{-2}$ and 61 $W \cdot m^{-2}$, respectively. Since the global convective flux prior to the Pleistocene should be like the present interglacial hence of O (100 $W \cdot m^{-2}$), and given the Pleistocene cooling of order 10 ^{0}C (Ruddiman and Raymo 1988, Fig. 3), the downward LW flux as well as the global convective flux can be reduced by 50 $W \cdot m^{-2}$ (Ou 2001, Fig. 2), so the above criteria of the EPT and MPT are readily met to support their explanation by the model.

The deduced three stages represent a shift of the power spectra from that dominated by the obliquity to the emergence of the precession to that dominated by the eccentricity, as indeed seen in the observed ones (Imbrie et al. 1993, Fig. 3; Berger 1988, Fig. 16; McClymont et al. 2012, Fig. 6, top panel). The emergence of the precession signal in Stage 2 would shorten the interglacial and enhance the saw-tooth asymmetry, which are among the defining features of the observed EPT (Lisiecki and Raymo 2007).

3.5 Timeseries

https://doi.org/10.5194/cp-2021-94
Preprint. Discussion started: 20 July 2021

For a visualization of the temporal signals, we next present timeseries calculated from the model for Stage 2 and 3 (no need to show Stage 1 characterized by interglacial signals linear in the obliquity forcing). We have argued in Sect. 3.1 that with the full operation of the ice-albedo feedback hence precession forcing, the model forcing can be approximated by the Milankovitch insolation, which is set to

$$q' = \bar{q}^t + \sum_{i=1}^{3} a_i \cos\ \omega_i t. \tag{10}$$

where the time-mean forcing (the cold-box deficit) is $\bar{q}^t$ =100 $W \cdot m^{-2}$, obliquity ($i = 1$) has a period of 41 ky and amplitude $a_1 = 10\ W \cdot m^{-2}$), and precessions ($i = 2$ and 3) have periods of 18.5 and 23 ky with amplitudes $a_2 = a_3 = 20\ W \cdot m^{-2}$, respectively, which renders a 21 ky precession modulated by 95 ky eccentricity. The total range of our forcing thus is 100 $W \cdot m^{-2}$, as is the observed Milankovitch insolation (Berger et al. 1996, Fig. 3a).

With the above forcing, our climate model discussed in Sect. 2 would produce (time-varying) equilibrium SST and ice margin, which are now subscripted "*e*" for distinction. To calculate the timeseries, we apply the relaxation equations:

$$dT'/dt = (T_e{}' - T')/\tau_T, \tag{11}$$

and

$$dl/dt = (l_e - l)/\tau_l \tag{12}$$

https://doi.org/10.5194/cp-2021-94
Preprint. Discussion started: 20 July 2021

where the time constant for temperature is the entropy adjustment time set at 1 ky and τ_l is the time constant for the ice margin, which we distinguish between its advance and retreat (Weertman 1964). The ice advance is limited by the accumulation: for a snowfall of 0.3 m/y for example (Ohmura and Reeh 1991), to build up an ice sheet to 3 km high takes about 10 ky, which is thus set to be the advance time constant. The ice retreat on the other hand can be much faster: for 2 degrees warming for example, the melt rate is 4 m/y (Pollard 1980), which is an order greater than the accumulation, we thus set the retreat time constant to be 1 ky. The relaxation equations being linear, using different time constants merely affects the lag of the curves but produces no material difference.

We show in Fig. 6 timeseries and power spectra of the forcing (solid line), the subpolar SST (dashed) and ice margin (dotted) for Stage 2 and 3 of Fig. 5 (the MATLAB script is provided in Appendix C). The initial condition is the warm MEP state and integration is carried forward for 400 ky; since the glacial cycles are largely repetitive, we plot only the last cycle, the power spectra are however calculated for the full 400-ky timeseries. The upper axis represents the global-mean absorbed flux and SST. The forcing, being referenced to the former, is expressed in its temperature equivalent (100 $W \cdot m^{-2}$, for example, would convert to 8 ^{0}C, see Appendix B), the global-mean SST is set to 14 ^0C, the ice margin is its fractional extension into the subpolar region, and the shaded bar indicates the bistable interval.

It is seen that the forcing timeseries resembles the observed Milankovitch insolation (Berger et al. 1996, Fig. 3a) and expectedly contains no power at the eccentricity period. The timeseries for Stage 2 (Fig. 6a) show that only one precession trough during high eccentricity

https://doi.org/10.5194/cp-2021-94
Preprint. Discussion started: 20 July 2021

Climate of the Past
Discussions

has exceeded the cold threshold to generate the glacial state characterized by freezing-point SST and an ice sheet extending about half-way into the subpolar. Other than this single glacial episode lasting half the precession period, the rest of the timeseries are the interglacial SST that tracks the forcing with slight delay and negligible ice-cap cycles. Given the short duration of the glacial state, the SST and ice-margin spectra show no appreciable power at the eccentricity period, consistent with the observed spectra (Imbrie et al. 1993, Fig. 3).

The timeseries of Stage 3 differs qualitatively from that of Stage 2. There are episodes of interglacial during high precession peaks, which however always revert to glacial state at the next precession trough and then there is only glacial state spanning the low eccentricity, its long duration allows the ice sheet to grow to mid-latitudes. Although the SST and ice-margin spectra retain the precession and obliquity peaks as Stage 2, they show a strong eccentricity peak absent in Stage 2. This sharp contrast is consistent with the observed spectra (Imbrie et al. 1993, Fig. 3).

The ice signal bears sufficient resemblance to the last ice age cycle to allow marking of the corresponding marine isotope stages (MIS), as indicated in the figure, whose observational features thus may be interpreted by the model physics. According to our model, the cold sub-stages are characterized by freezing-point subpolar water, which is consistent with the ob-served expansion of the polar watermass and appearance of the polar species (McManus et al. 1994). Being a glacial state, the ice growth to the mid-latitudes is only limited by the duration of the half precession period, which has nonetheless reached half-way to the subtropical front. This modelled ice sheet is consistent with its observational estimate (Ruddiman et al. 1980;

https://doi.org/10.5194/cp-2021-94
Preprint. Discussion started: 20 July 2021

Chapman and Shackleton 1999), which is also supported by Ice-rafted debris (IRD) events preconditioned on a large ice sheet (McManus et al. 1994). In our interpretation, all substages are generically similar with the glacial at the cold substages reversed by the next precession peak to the interglacial warm substages, as seen in their comparable temperature (Berger 1979, Fig. 8). It is the MIS 4 that represents the onset of the ice age (Ruddiman et al. 1980) as the succeeding precession peak fails to clear the warm threshold, resulting in prolonged coldness and an ice sheet extending to mid-latitudes as manifested in the LIS. It is noted that the ice margin is saw-toothed even within one precession trough due solely to the disparate advance and retreat rates, and this asymmetry is strongly amplified for the ice ages due to the ice growth through the low eccentricity before the abrupt ice retreat**.**

4 Discussion

The central tenet of our theory is that the ocean is the intermediary of the orbital forcing of the global ice, as strongly argued by Broecker and Denton (1989). Since the ocean is heated by the annual absorbed flux integrated over the subpolar water, it naturally filters out latitudinal difference of the obliquity and precession forcing --- except the latter would become effective when the ice-albedo feedback is activated during the Pleistocene cooling. As such, the forcing is dominated by the obliquity component in the early Pleistocene, but can be approximated by the Milankovitch insolation in the late Pleistocene. The use of the latter in our model thus is not because of its direct effect on the summer SAT and ablation, but because it mimics the late-Pleistocene forcing of the ocean.

https://doi.org/10.5194/cp-2021-94
Preprint. Discussion started: 20 July 2021

While there can be inherent bistability of finite ice sheet and ice-free state (Weertman 1961), we argue that the ice-free state is untenable in Pleistocene with the emergence of the Arctic perennial ice about 3 Ma, as also attested by the current Greenland ice sheet and the substantial obliquity signal even in the early Pleistocene. Rather, we posit that bistability of the ice simply reflects that of the subpolar ocean, which in a coupled and NT climate system may exhibit bistable warm and freezing-point temperature. Through its effect on the summer SAT that controls the ice margin, this bistability would translate to that of the ice characterized by polar ice cap and an ice sheet extending to mid-latitudes. The vast difference of these ice bistates produces strong ice signal regardless the forcing perturbation so long as the bistable thresholds are crossed.

The bistable interval of the coupled climate is linked to the global convective flux, which would be lowered during the Pleistocene cooling that produces drier atmosphere; its interplay with the ice-albedo feedback leads to three stages of the ice cycles, as well discerned in observations (Imbrie et al. 1993; Lisiecki and Raymo 2007). In the warm early Pleistocene before appreciable ice-albedo feedback hence the precession forcing, the ice cycles are simply that of the polar ice cap perturbed linearly by the obliquity (Stage 1). The continuing cooling would enhance the ice-albedo feedback hence the precession forcing; while the precession troughs during high eccentricity may induce the glacial state, it is nullified by the next precession peak, resulting in G/IG cycle at the precession period (Stage 2). With further cooling, the precession peaks may no longer clear the warm threshold, so the glacial state would last through the low eccentricity, resulting in ice-age cycles paced by the eccentricity (Stage 3).

https://doi.org/10.5194/cp-2021-94
Preprint. Discussion started: 20 July 2021

The transitions between the three stages correspond to the EPT and MPT discerned in Lisiecki and Raymo (2007), which are now assigned specific markers that can be crossed during the Pleistocene cooling.

It should be noted that in our formulation, there are only bistable glacial and interglacial states, the ice age is merely the glacial state that lasts through low eccentricity, there is no need for a third full-glacial state as posited by Paillard (1998), who has not provided dynamical basis for such a state nor the transition rules among his tri-states. Since an interactive MOC is key to the ocean bistability, numerical models that fix the SST or assume a slab ocean (North et al. 1983; Abe-Ouchi et al. 2013) obviously cannot capture the ocean effect on the climate. While coarse-grained coupled models have produced ocean hysteresis (Rahmstorf et al. 2005), it is opposite in sign to that of the glacial cycle, the reason being, without resolving eddies, the MOC is constrained by a fixed diapycnal diffusivity (Sect. 2.1). Deprived of the proper ocean hysteresis, numerical calculations of the glacial cycles are compelled to prescribe a CO_2 trend or an orbital-period CO_2 in augmenting the glacial signal (Berger et al. 1999; Ganopolski and Calov 2011; Willeit et al. 2019) --- both need further justification (Sect. 1). To properly constrain the MOC requires resolving ocean eddies, which poses a daunting challenge to numerical models because of the long time-integration needed, but a phenomenological approach of coding the entropy production tendency, say, via a variable eddy diffusivity, may remain feasible.

5 Resolving glacial puzzles

https://doi.org/10.5194/cp-2021-94
Preprint. Discussion started: 20 July 2021

Our theory provides a single dynamic framework that may resolve seemingly unrelated Pleistocene puzzles of the glacial cycles, as further expounded below. The reason that there is only 41-ky obliquity cycles in the early Pleistocene is because, without the ice-albedo feedback, the precession has no effect on the annual absorbed flux on account of the Kepler's law, our theory thus may resolve the "41-ky" problem. That such flux being the relevant forcing has rendered moot some previous solutions to the 41-ky problem, such as Raymo and Nisancioglu (2003) or Raymo and Huybers (2008). The MPT to the 100-ky ice-age cycle occurs when the Pleistocene cooling has allowed the glacial state to last through the low eccentricity hence paced by the latter; its strong signal is caused by disparate ice bistates between the polar ice cap and an ice sheet extending to mid-latitudes; our model thus may resolve the "100-ky" problem.

So long as the ice-age pacing is enabled by the shorter period 100-ky eccentricity, the strength of the ice-age cycle is no longer affected by the 400-ky eccentricity even though it has greater amplitude (Berger and Loutre 1991, Fig. 4a), the theory thus may resolve the "400-ky" problem (Imbrie et al. 1993; Berger and Loutre 2010). In fact, it is seen from Fig. 5 that a smaller eccentricity would produce a longer-lasting ice age to augment the ice signal, which may explain why the 100-ky signal is gaining strength when the eccentricity is decreasing (Clark et al. 1999, Fig. 6b) or why the lower eccentricity at Stage 11 is accompanied by higher 100-ky signal; the latter often dubbed the "Stage-11" problem (Imbrie et al. 1993, Fig. 2).

Since the onset and termination of the ice ages are threshold phenomena, both can be off by one precession period depending on the precise timing, the ice-age cycles thus may vary

https://doi.org/10.5194/cp-2021-94
Preprint. Discussion started: 20 July 2021

between 80- and 120-ky (Raymo et al. 1997) to resolve the “variable termination” problem. Since the summer insolation anomalies are out-of-phase between hemispheres, their synchronous glacial cycles have posed a significant puzzle (Broecker and Denton 1989), but since the relevant orbital forcing is the annual absorbed flux, it has naturally removed this hemispheric difference. Then with the northern ice sheet dominating the response, it would feed back onto the global balance to synchronize the Antarctic climate, as suggested by the latter’s slight lag (a few millennia) from the Milankovitch insolation (Kawamura et al. 2007); the model thus may possibly resolve this “polar synchronization” problem.

Appendix A: Acronyms

EL	Equilibrium line
ELA	Equilibrium-line altitude
EPT	Early Pleistocene transition
G/IG	Glacial/interglacial
IRD	Ice-rafted debris
Ka	Thousand years ago
Ky	Thousand years
LGM	Last glacial maximum
LIS	Laurentide ice sheet
LW	Long-wave
Ma	Million years ago
MEP	Maximum entropy production

https://doi.org/10.5194/cp-2021-94
Preprint. Discussion started: 20 July 2021

MIS Marine isotope stage

MOC Meridional overturning circulation

MPT Mid-Pleistocene transition

NT Nonequilibrium thermodynamics

SAT Surface-air temperature

SST Sea-surface temperature

SW Short-wave

Appendix B: Symbols and standard values

A_b Ablation rate

A_c Accumulation rate (= $2 \times 10^5 m^2/y$)

$C_{p,o}$ Specific heat of ocean (= $4.2 \times 10^3 J\ Kg^{\ -1} K^{-1}$)

g Gravitational acceleration (= $9.8\ m \cdot s^{-2}$)

h Ice-surface height

h_0 ELA

K Mass exchange rate of MOC

$[K]$ Scale of K (= $\alpha^* L (2\rho_o C_{p,o})^{-1} = 4.5 m^2/s$)

l x-coordinate of ice margin

l_e Equilibrium l

l_0 x-coordinate of ELA

L Latitudinal span of cold box (= $3 \times 10^3 km$)

https://doi.org/10.5194/cp-2021-94
Preprint. Discussion started: 20 July 2021

Climate of the Past Discussions

q'	Cold-box deficit of absorbed solar flux
$\bar{q}^t$	Long-term mean of q' ($= 100\ W \cdot m^{-2}$)
$[q']$	scale of q' ($= \bar{q}^t = 100\ W \cdot m^{-2}$)
$\bar{q}_c'$	Global convective flux
a_i	Amplitudes of Milankovitch insolation
q_c'	Cold-transition threshold
q_w'	Warm-transition threshold
S'	Cold-box salinity deficit
$[S']$	Scale of $S'(= \alpha[T']/\beta$=1.79)
$\bar{T}$	Global-mean SST ($= 14^0C$)
T'	Cold-box SST deficit
$[T']$	Scale of $T'(= [q']/\ \alpha^* = 8^0C)$
$T_a{}'$	Cold-box SAT deficit (from global-mean SST)
$T_e{}'$	Equilibrium T'
$T_f{}'$	Freezing-point temperature
T_i	Ice surface temperature
α	Thermal expansion coefficient ($= 1.7 \times 10^{-4} \cdot {}^0C^{-1}$)
α^*	Surface transfer coefficient ($= 12.5\ W \cdot m^{-2} \cdot {}^0C^{-1}$, Ou 2018)
β	Saline contraction coefficient ($= 7.6 \times 10^{-4}$)
γ	Lapse rate ($= 6^0C/km$)
ρ'	Cold-box density surplus

https://doi.org/10.5194/cp-2021-94
Preprint. Discussion started: 20 July 2021

$[\rho']$ Scale of ρ' ($= \rho_o \alpha [T'] = 1.36\ Kg \cdot m^{-3}$)

ρ_i Ice density ($= 0.9 \times 10^3\ Kg \cdot m^{-3}$)

ρ_o Ocean density ($= 10^3\ Kg \cdot m^{-3}$)

τ_i Yield stress ($= 1\ bar$)

τ_l Ice-sheet time constant ($= 1/10\ ky$ for retreat/advance)

τ_T MEP-adjustment time ($= 1\ ky$)

μ Moisture-content parameter ($= 0.3$)

ν Ice-melt parameter ($= 1.6\ m \cdot y^{-1} \cdot {}^0C^{-1}$)

Appendix C: MATLAB script

```
% assign parameters
dt=1;tmax=400;t=(0:dt:tmax);m=length(t);m2=m/2;
fre1=2*pi/41;fre2=2*pi/18.5;fre3=2*pi/23;
amp1=0.8;amp2=1.6;amp3=1.6;
pha1=0;pha2=0;pha3=0;
dtemp1=4.5;qmean=8;dtemp2=2*dtemp1;
tempf=14;temprange=10;
tausst=1;tauac=10;tauab=1;
gamma=0.3;
% set arrays
sste=zeros(1,m);sst=zeros(1,m);
icee=zeros(1,m);ice=zeros(1,m);
qprime=zeros(1,m);q=zeros(1,m);
% initialize with interglacial state (ig)
ig=true;
for i=1:(m-1)
   %insolation
   qprime(i)=amp1*cos(fre1*t(i)+pha1)...
      +amp2*cos(fre2*t(i)+pha2)...
      +amp3*cos(fre3*t(i)+pha3);
   q(i)=qmean-qprime(i);
   %calculate equilibrium temperature and ice margin
   if ig
      sste(i)=q(i);
      slt1=q(i)/2+dtemp1;
```

https://doi.org/10.5194/cp-2021-94
Preprint. Discussion started: 20 July 2021

Climate of the Past Discussions

```
      icee(i)=1-(tempf-slt1)/temprange;
      if q(i)>=dtemp2
        ig=false;
      end
   end
   if ~ig
      sste(i)=tempf;
      icee(i)=1;
      if q(i)<=(1+gamma)*dtemp1
        ig=true;
      end
   end
      %time integration using runge-kutta scheme
      sst(1)=sste(1);ice(1)=icee(1);
      sst(i+1)=runge(sste(i),sst(i),dt,tausst);
      ice(i+1)=rungeice(icee(i),ice(i),dt,tauac,tauab);
end
%rescale ice margin
ice5=5*(1-ice);
ice10=10*ice;
q=tempf-q;
sst=tempf-sst;
figure
% plot timeseries
subplot(2,1,1)
plot(t,q,'-k',t,sst,'--k',t,ice5,':k')
axis([60,170,0,tempf])
set(gca,'XDir','reverse');
%legend('q','sst','ice5','location','southeast')
title({['gla6a:','amp1=',num2str(amp1),',amp2=',num2str(amp2),...
   ',amp3=',num2str(amp3),',pha1=',num2str(pha1),...
   ',pha2=',num2str(pha2),',pha3=',num2str(pha3)];...
   ['dtemp1=',num2str(dtemp1),',qmean=',num2str(qmean),...
   ',temprange=',num2str(temprange),',tauac=',num2str(tauac),',tauab=',num2str(tauab),...
   ',gamma=',num2str(gamma)]})
xlabel('t (ky)');ylabel('temp')
% plot power spectra
yq=fft(qprime);
yq=fftshift(yq);
sstprime=sst-mean(sst);
ysst=fft(sstprime);
ysst=fftshift(ysst);
iceprime=ice10-mean(ice10);
```

https://doi.org/10.5194/cp-2021-94
Preprint. Discussion started: 20 July 2021

Climate of the Past
Discussions

```
yice=fft(iceprime);
yice=fftshift(yice);
f=(-m/2:m/2-1)/(dt*m);
powerq=2*abs(yq).^2/(m*m);
powersst=2*abs(ysst).^2/(m*m);
powerice=2*abs(yice).^2/(m*m);
subplot(2,1,2)
plot(f,powerq,'-k',f,powersst,'--k',f,powerice,':k')
axis([0,0.1,0,3])
legend('q','sst','ice')
xlabel('freq (cycles/ky)');ylabel('power')

% runge-kutta scheme for sst
function y=runge(x,r,dt,tau)
    heating=@(r) (x-r)/tau;
    k1 = heating(r);
    k2 = heating(r+0.5*dt*k1);
    k3 = heating(r+0.5*dt*k2);
    k4 = heating(r+dt*k3);
    y = r+1/6*dt*(k1+2*k2+2*k3+k4);

% runge-kutta scheme for ice margin
function y=rungeice(x,r,dt,tauac,tauab)
    msign=x-r;
    if msign<0
      tau=tauab;
    else
      tau=tauac;
    end
    mbalance=@(r) (x-r)/tau;
    k1 = mbalance(r);
    k2 = mbalance(r+0.5*dt*k1);
    k3 = mbalance(r+0.5*dt*k2);
    k4 = mbalance(r+dt*k3);
    y = r+1/6*dt*(k1+2*k2+2*k3+k4);
```

References

https://doi.org/10.5194/cp-2021-94
Preprint. Discussion started: 20 July 2021

Abe-Ouchi A, Saito F, Kawamura K, Raymo ME, Okuno JI, Takahashi K, Blatter H (2013) Insolation-driven 100,000-year glacial cycles and hysteresis of ice-sheet volume. Nature 500(7461):190-193 https://doi.org/10.1038/nature12374

Alley RB, Clark PU, Keigwin LD, Webb RS (1999) Making sense of millennial-scale climate change. Geophys Monogr-AGU 112:385-94 https://doi.org/10.1029/gm112p0385

Berger A (1979) Spectrum of climatic variations and their causal mechanisms. Geophys Surveys 3(4), 351-402 https://doi.org/10.1007/bf01449756

Berger A (1988) Milankovitch theory and climate. Rev Geophys 26(4):624-57 https://doi.org/10.1029/rg026i004p00624

Berger A, Gallee H, Li XS, Dutrieux A, Loutre MF (1996) Ice sheet growth and high-latitudes sea surface temperature. Clim Dyn 12:441–448 https://doi.org/10.1007/s003820050119

Berger A, Li X, Loutre M (1999) Modeling northern hemisphere ice volume over the last 3 ma. Quat Sci Rev 18:1 – 11 https://doi.org/10.1016/s0277-3791(98)00033-x

Berger A, Loutre MF (1991) Insolation values for the climate of the last 10 million years. Quat Sci Rev 10(4):297-317 https://doi.org/10.1016/0277-3791(91)90033-q

Berger A, Loutre MF (2010) Modeling the 100-kyr glacial–interglacial cycles. Global Planet Change 72(4):275-81 https://doi.org/10.1016/j.gloplacha.2010.01.003

https://doi.org/10.5194/cp-2021-94
Preprint. Discussion started: 20 July 2021

Berger A, Loutre MF, Kaspar F, Lorenz SJ (2007) Chapter 2. Insolation during interglacial. In Developments in Quaternary Sciences (Vol. 7, 13-27), Elsevier https://doi.org/10.1016/s1571-0866(07)80027-3

Broecker WS (1994) Massive iceberg discharges as triggers for global climate change. Nature 372:421-4 https://doi.org/10.1038/372421a0

Broecker WS, Denton GH (1989) The role of ocean-atmosphere reorganization in glacial cycles. Geochim Cosmochim Acta 53:2465-501 https://doi.org/10.1016/0016-7037(89)90123-3

Broecker WS, Peteet DM, Rind D (1985) Does the ocean-atmosphere system have more than one stable mode of operation? Nature 315 (6014):21-6 https://doi.org/10.1038/315021a0

Calov R, Ganopolski A (2005) Multistability and hysteresis in the climate-cryosphere system under orbital forcing. Geophys Res Lett 32:L21717 https://doi.org/10.1029/2005gl024518

Chapman MR and Shackleton NJ (1999) Global ice-volume fluctuations, North Atlantic ice-rafting events, and deep-ocean circulation changes between 130 and 70 ka. Geology 27, 795–8 https://doi.org/10.1130/0091-7613(1999)027<0795:givfna>2.3.co;2

Clark DL (1982) Origin, nature and world climate effect of Arctic Ocean ice-cover. Nature 300(5890):321-5 https://doi.org/10.1038/300321a0

https://doi.org/10.5194/cp-2021-94
Preprint. Discussion started: 20 July 2021

Climate of the Past Discussions

Clark PU, Alley RB, Pollard D (1999) Northern Hemisphere ice sheet influences on global climate change. Science 286:1104–11 https://doi.org/10.1126/science.286.5442.1104

Clark, PU, Archer D, Pollard D, Blum JD, Rial JA, Brovkin V, Mix AC, Pisias NG, Roy M (2006) The middle Pleistocene transition: characteristics, mechanisms, and implications for long-term changes in atmospheric pCO2. Quat Sci Rev 25:3150-84 https://doi.org/10.1016/j.quascirev.2006.07.008

CLIMAP PM (1976) The surface of the ice-age earth. Science 191(4232):1131-7 https://doi.org/10.1126/science.191.4232.1131

Crooks GE (1999) Entropy production fluctuation theorem and the nonequilibrium work relation for free energy differences. Phys Rev E 60(3):2721-6 https://doi.org/10.1103/physreve.60.2721

Crucifix M (2013) Why could ice ages be unpredictable? Clim Past (9):2253-67 https://doi.org/10.5194/cp-9-2253-2013

Daruka I, Ditlevsen PD (2016) A conceptual model for glacial cycles and the middle Pleistocene transition. Clim Dyn (46):29-40 https://doi.org/10.1007/s00382-015-2564-7

Denton GH, Anderson RF, Toggweiler JR, Edwards RL, Schaefer JM, Putnam AE (2010) The last glacial termination. Science 328(5986):1652-6 https://doi.org/10.1126/science.1184119

https://doi.org/10.5194/cp-2021-94
Preprint. Discussion started: 20 July 2021

Donohoe A, Battisti DS (2013) The seasonal cycle of atmospheric heating and temperature. J Clim 26(14):4962-80 https://doi.org/10.1175/jcli-d-12-00713.1

Duplessy JC, Labeyrie L, Arnold M, Paterne M, Duprat J, van Weering TC (1992) Changes in surface salinity of the North Atlantic Ocean during the last deglaciation. Nature 358(6386):485-8 https://doi.org/10.1038/358485a0

Elkibbi M, Rial JA (2001) An outsider's review of the astronomical theory of the climate: is the eccentricity-driven insolation the main driver of the ice ages? Earth Sci Rev 56(1-4):161-77 https://doi.org/10.1016/s0012-8252(01)00061-7

Ganopolski A, Calov R (2011) The role of orbital forcing, carbon dioxide and regolith in 100 kyr glacial cycles. Clim Past 7:1415-25 https://doi.org/10.5194/cp-7-1415-2011

Ghil M (1994) Cryothermodynamics: The chaotic dynamics of paleoclimate. Physica D 77:130–59 https://doi.org/10.1016/0167-2789(94)90131-7

Gildor H, Tziperman E (2003) Sea-ice switches and abrupt climate change. Philos Trans R Soc London Ser A 361(1810):1935-44 https://doi.org/10.1098/rsta.2003.1244

Hays JD, Imbrie J, Shackleton NJ (1976) Variations in the Earth's orbit: pacemaker of the ice ages. Science 194(4270):1121-32 https://doi.org/10.1126/science.194.4270.1121

https://doi.org/10.5194/cp-2021-94
Preprint. Discussion started: 20 July 2021

Honisch B, Hemming NG, Archer D, Siddall M, McManus JF (2009) Atmospheric carbon dioxide concentration across the mid-Pleistocene transition. Science 324:1551-4 https://doi.org/10.1126/science.1171477

Huybers P (2006) Early Pleistocene glacial cycles and the integrated summer insolation forcing. Science 313(5786):508-11 https://doi.org/10.1126/science.1125249

Imbrie J, Berger A, Boyle E, Clemens SC, Duffy A, Howard WR, Kukla G, Kutzbach J, Martinson DG, McIntyre A, Mix AC, Molfino B, Morley JJ, Peterson LC, Pisias NG, Prell WL, Raymo ME, Shackleton NY, Toggweiler JR (1993) On the structure and origin of major glaciation cycles 2. The 100,000-year cycle. Paleoceanogr 8(6):699-735 https://doi.org/10.1029/93pa02751

Imbrie J, Boyle EA, Clemens SC, Duffy A, Howard WR, Kukla G, Kutzbach J, Martinson DG, McIntyre A, Mix AC, Molfino B (1992) On the structure and origin of major glaciation cycles 1. Linear responses to Milankovitch forcing. Paleoceanogr 7(6):701-38 https://doi.org/10.1029/92pa02253

Imbrie J, Imbrie JZ (1980) Modeling the Climatic Response to Orbital Variations. Science 207:943-53 https://doi.org/10.1126/science.207.4434.943

Imbrie JZ, Imbrie-Moore A, Lisiecki LE (2011) A phase-space model for Pleistocene ice volume. Earth Planet Sci Lett 307(1-2):94-102 https://doi.org/10.1016/j.epsl.2011.04.018

Kawamura K, Parrenin F, Lisiecki L, Uemura R, Vimeux F, Severinghaus JP, Hutterli MA, Nakazawa T, Aoki S, Jouzel J, Raymo ME (2007) Northern Hemisphere forcing of climatic cycles in Antarctica over the past 360,000 years. Nature 448(7156):912-6 https://doi.org/10.1038/nature06015

Keigwin LD, Curry WB, Lehman SJ, Johnsen S (1994) The role of the deep ocean in North Atlantic climate change between 70 and 130 kyr ago. Nature 371(6495):323-6 https://doi.org/10.1038/371323a0

Kleidon A (2009) Non-equilibrium thermodynamics and maximum entropy production in the Earth system: applications and implications. Naturwiss 96:653–77 https://doi.org/10.1007/s00114-009-0509-x

Letreguilly A, Huybrechts P, Reeh N (1991) Steady-state characteristics of the Greenland ice sheet under different climates. J Glaciol 37(125):149-57 https://doi.org/10.1017/s0022143000042908

Lisiecki LE (2010) Links between eccentricity forcing and the 100,000-year glacial cycle. Nature Geos 3:349-52 https://doi.org/10.1038/ngeo828

Lisiecki LE, Raymo ME (2007) Plio–Pleistocene climate evolution: trends and transitions in glacial cycle dynamics. Quat Sci Rev 26(1):56-69 https://doi.org/10.1016/j.quascirev.2006.09.005

https://doi.org/10.5194/cp-2021-94
Preprint. Discussion started: 20 July 2021

Lisiecki LE, Raymo ME, Curry WB (2008) Atlantic overturning responses to Late Pleistocene climate forcings. Nature 456:85-8 https://doi.org/10.1038/nature07425

Macdonald A M (1998) The global ocean circulation: A hydrographic estimate and regional analysis. Progr Oceanogr 41(3):281-382 https://doi.org/10.1016/s0079-6611(98)00020-2

Manabe S, Stouffer RJ (1988) Two stable equilibria of a coupled ocean-atmosphere model. J Clim 1:841-66 https://doi.org/10.1175/1520-0442(1988)001<0841:tseoac>2.0.co;2

Marotzke J, Stone P (1995) Atmospheric transports, the thermohaline circulation, and flux adjustments in a simple coupled model. J Phys Oceanogr 25:1350-64 https://doi.org/10.1175/1520-0485(1995)025<1350:atttca>2.0.co;2

McClymont E, Sodian S, Rosell-Mele A, Rosenthal Y (2013) Pleistocene sea-surface temperature evolution: early cooling, delayed glacial intensification, and implications for the mid-Pleistocene climate transition. Earth Sci Rev 123:173–93 https://doi.org/10.1016/j.earscirev.2013.04.006

McManus JF, Bond GC, Broecker WS, Johnsen S, Labeyrie L, Higgins S (1994) High-resolution climate records from the N. Atlantic during the last interglacial. Nature 371:326–9 https://doi.org/10.1038/371326a0

Medina-Elizalde M, Lea DW (2005) The mid-Pleistocene transition in the tropical Pacific. Science 310(5750):1009-12 https://doi.org/10.1126/science.1115933

https://doi.org/10.5194/cp-2021-94
Preprint. Discussion started: 20 July 2021

Climate of the Past Discussions

Meyers SR, Hinnov L (2010) Northern hemisphere glaciation and the evolution of Plio-Pleistocene climate noise. Paleoceanogr 25:PA3207 https://doi.org/10.1029/2009pa001834

Milankovitch M (1941) Canon of insolation and the ice-age problem. R Serb Acad Spec Publ 132 (Translated from German, Israel Program for Scientific Translations) Jerusalem, 1969

Nie J, King J, Fang X (2008) Late Pliocene-early Pleistocene 100-ka problem. Geophys Res Lett 35:L21606 https://doi.org/10.1029/2008gl035265

North GR, Mengel JG, Short DA (1983) Simple energy balance model resolving the seasons and the continents: Application to the astronomical theory of the ice ages. J Geophys Res 88(C11):6576-86 https://doi.org/10.1029/jc088ic11p06576

Oerlemans J (1980) On zonal asymmetry and climate sensitivity. Tellus 32(6):489-99 https://doi.org/10.3402/tellusa.v32i6.10604

Oerlemans J (1982) Glacial cycles and ice-sheet modelling. Clim Change 4(4):353-74 https://doi.org/10.1007/bf02423468

Oerlemans J (1991) The mass balance of the Greenland ice sheet: sensitivity to climate change as revealed by energy-balance modelling. Holocene 1(1):40-8 https://doi.org/10.1177/095968369100100106

https://doi.org/10.5194/cp-2021-94
Preprint. Discussion started: 20 July 2021

Climate of the Past Discussions

Ohmura A, Reeh N (1991) New precipitation and accumulation maps for Greenland. J Glaciol 37(125):140-8 https://doi.org/10.3189/s0022143000042891

Ou HW (2001) Possible bounds on the earth's surface temperature: From the perspective of a conceptual global-mean model. J Clim 14:2976-88 https://doi.org/10.1175/1520-0442(2001)014<2976:pbotes>2.0.co;2

Ou HW (2007) Hydrological cycle and ocean stratification in a coupled climate system: a theoretical study. Tellus 59A:683-94 https://doi.org/10.3402/tellusa.v59i5.15157

Ou HW (2018) Thermohaline circulation: a missing equation and its climate change implications. Clim Dyn 50:641–53 https://doi.org/10.1007/s00382-017-3632-y

Ozawa H, Ohmura A, Lorenz RD, Pujol T (2003) The second law of thermodynamics and the global climate system: A review of the maximum entropy production principle. Rev Geophys 41:4/10182003 https://doi.org/10.1029/2002rg000113

Paillard D (1998) The timing of Pleistocene glaciations from a simple multiple-state climate model. Nature 391:378-81 https://doi.org/10.1038/34891

Peixoto JP, Oort AH (1992) Physics of Climate. Amer Inst Phys, New York https://doi.org/10.1063/1.2809772

Pelletier JD (2003) Coherence resonance and ice ages. J Geophys Res 108(D20):4645 https://doi.org/10.1029/2002jd003120

https://doi.org/10.5194/cp-2021-94
Preprint. Discussion started: 20 July 2021

Petit JR, Jouzel J, Raynaud D, Barkov NI, Barnola JM, Basile I, Bender M, Chappellaz J, Davis M, Delaygue G, Delmotte M (1999) Climate and atmospheric history of the past 420,000 years from the Vostok ice core, Antarctica. Nature 399(6735):429-36 https://doi.org/10.1038/20859

Pollard D (1980) A simple parameterization for ice sheet ablation rate. Tellus 32(4):384-8 https://doi.org/10.1111/j.2153-3490.1980.tb00965.x

Pollard D (1983) A coupled climate-ice sheet model applied to the Quaternary ice ages. J Geophys Res 88(C12):7705-18 https://doi.org/10.1029/jc088ic12p07705

Rahmstorf S, Crucifix M, Ganopolski A, Goosse M, Kamenkovich I, Knutti R, Lohmann G, Marsh R, Mysak LA, Wang Z, Weaver AJ (2005) Thermohaline circulation hysteresis: A model intercomparison. Geophys Res Lett 32(23) L23605, https://doi.org/10.1029/2005gl023655

Ravelo AN, Andreasen DH, Lyle M, Lyle AO, Wara MW (2004) Regional climate shifts caused by gradual global cooling in the Pliocene epoch. Nature 429:263-7 https://doi.org/10.1038/nature02567

Raymo ME (1997) The timing of major climate terminations. Paleoceanogr 12(4):577-85 https://doi.org/10.1029/97pa01169

Raymo ME, Huybers P (2008) Unlocking the mysteries of the ice ages. Nature 451(7176):284-5 https://doi.org/10.1038/nature06589

https://doi.org/10.5194/cp-2021-94
Preprint. Discussion started: 20 July 2021

Raymo ME, Nisancioglu KH (2003) The 41 kyr world: Milankovitch's other unsolved mystery. Paleoceanogr 18(1) https://doi.org/10.1029/2002pa000791

Raymo ME, Oppo DW, Curry W (1997) The mid-Pleistocene climate transition: a deep sea carbon isotopic perspective. Paleoceanogr 12(4):546-59 https://doi.org/10.1029/97pa01019

Ruddiman WF, McIntyre A, Niebler-Hunt V, Durazzi JT (1980) Oceanic evidence for the mechanism of rapid northern hemisphere glaciation. Quat Res 13(1):33-64 https://doi.org/10.1016/0033-5894(80)90081-2

Ruddiman W, Raymo M (1988) Northern Hemisphere climate regimes during the past 3 Ma: Possible tectonic connections. Phil Trans R Soc London Ser B 318:411-30 https://doi.org/10.1098/rstb.1988.0017

Ruddiman WF, Shackleton NJ, McIntyre A (1986) North Atlantic sea-surface temperatures for the last 1.1 million years. Geol Soc, London, Spec pub 21(1):155-73 https://doi.org/10.1144/gsl.sp.1986.021.01.11

Saltzman B, Hansen A, Maasch K (1984) The late Quaternary glaciations as the response of a three-component feedback system to Earth-orbital forcing. J Atmos Sci 41:3380–9 https://doi.org/10.1175/1520-0469(1984)041<3380:tlqgat>2.0.co;2

https://doi.org/10.5194/cp-2021-94
Preprint. Discussion started: 20 July 2021

Shackleton N (2000) The 100,000-year ice-age cycle identified and found to lag temperature, carbon dioxide, and orbital eccentricity. Science 289:1897– 902 https://doi.org/10.1126/science.289.5486.1897

Siegenthaler U, Stocker TF, Monnin E, Lüthi D, Schwander J, Stauffer B, Raynaud D, Barnola JM, Fischer H, Masson-Delmotte V, Jouzel J (2005) Stable carbon cycle–climate relationship during the late Pleistocene. Science 310(5752):1313-7 https://doi.org/10.1126/science.1120130

Stommel H (1961) Thermohaline convection with two stable regimes of flow. Tellus 13:224-30 https://doi.org/10.1111/j.2153-3490.1961.tb00079.x

Tricot C, Berger A (1988) Sensitivity of present-day climate to astronomical forcing. In *Long and Short Term Variability of Climate* (p. 132-52), Springer Berlin Heidelberg https://doi.org/10.1007/bfb0046593

Tziperman E, Raymo ME, Huybers PJ, Wunsch C (2006) Consequences of pacing the Pleistocene 100 kyr ice ages by nonlinear phase locking to Milankovitch forcing. Paleoceanogr 21(PA4206):1-11 https://doi.org/10.1029/2005pa001241

Van der Veen CI (2013) Fundamentals of glacier dynamics, CRC Press (second edition), Boca Raton, FL, 403 pp. https://doi.org/10.1201/b14059

Weertman J (1961) Stability of ice-age ice sheets. J Geophys Res 66(11):3783-92 https://doi.org/10.1029/jz066i011p03783

https://doi.org/10.5194/cp-2021-94
Preprint. Discussion started: 20 July 2021

Climate of the Past
Discussions

Weertman J (1964) Rate of growth or shrinkage of nonequilibrium ice sheets. J Glaciol 5(38):145-58 https://doi.org/10.3189/s0022143000028744

Weertman J (1976) Milankovitch solar radiation variations and ice age ice sheet sizes. Nature 261:17-20 https://doi.org/10.1038/261017a0

Wunsch C (2003) The spectral description of climate change including the 100 ky energy. Clim Dyn 20(4):353-63 https://doi.org/10.1007/s00382-002-0279-z

https://doi.org/10.5194/cp-2021-94
Preprint. Discussion started: 20 July 2021

Climate of the Past
Discussions

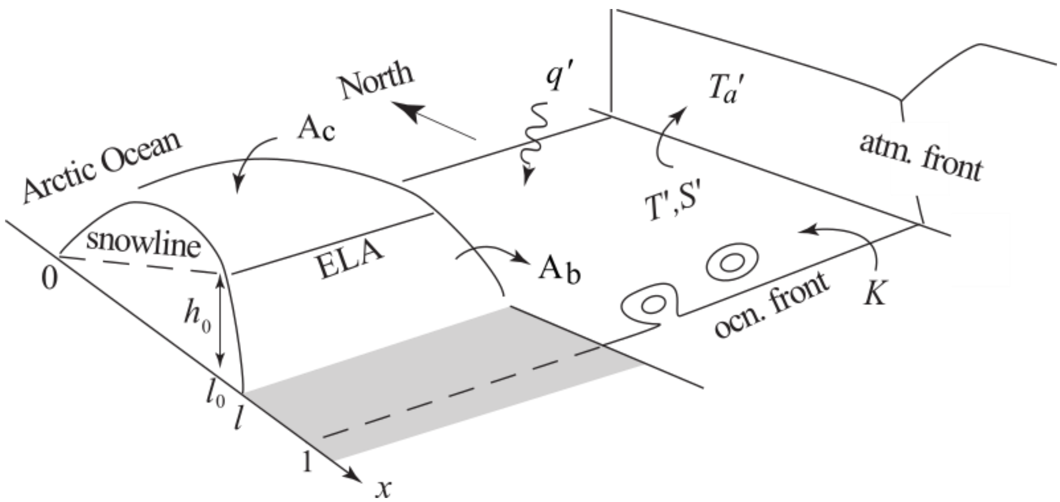

Figure 1: The model configuration of coupled ocean/atmosphere composed of warm and cold boxes aligned at mi-latitudes and an ice sheet on a continental strip terminated at the Arctic Ocean. The prognostic variables include the cold-box deviations from global means, the MOC, and the ice margin (all symbols are listed in Appendix B)

https://doi.org/10.5194/cp-2021-94
Preprint. Discussion started: 20 July 2021

Climate of the Past
Discussions

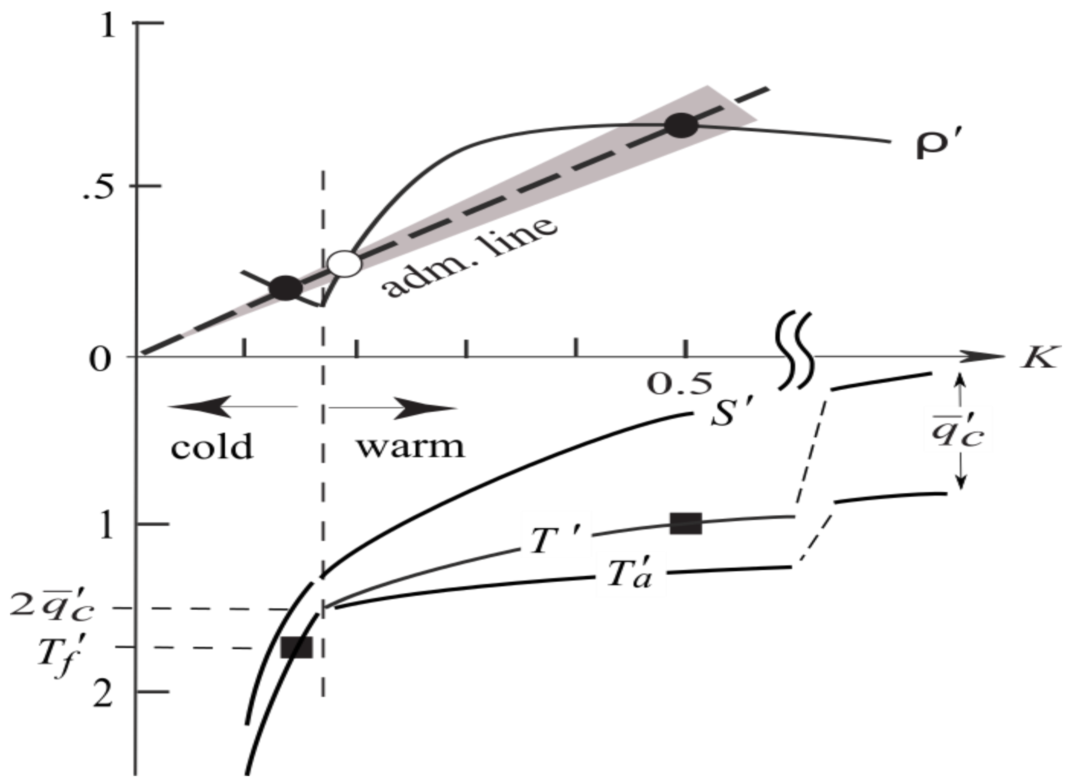

Figure 2: The regime diagram in which the cold-box deviations (solid lines) from the global-means (the horizontal axis) are plotted against the MOC (K). The vertical dashed line marks the convective bound when the convective flux vanishes, which divides the warm and cold branches. The intersects of the admittance line (thick dashed) with the density curve specifies the climate state (solid ovals). Subjected to fluctuations (shaded cone), the admittance line would pivot toward the MEP states (solid rectangles), which define the interglacial and glacial states, the latter characterized by the freezing-point but ice-free subpolar water. The graph is for the case of $q' = 1$, $\bar{q}_c' = .75$, and $T_f' = 1.75$

https://doi.org/10.5194/cp-2021-94
Preprint. Discussion started: 20 July 2021

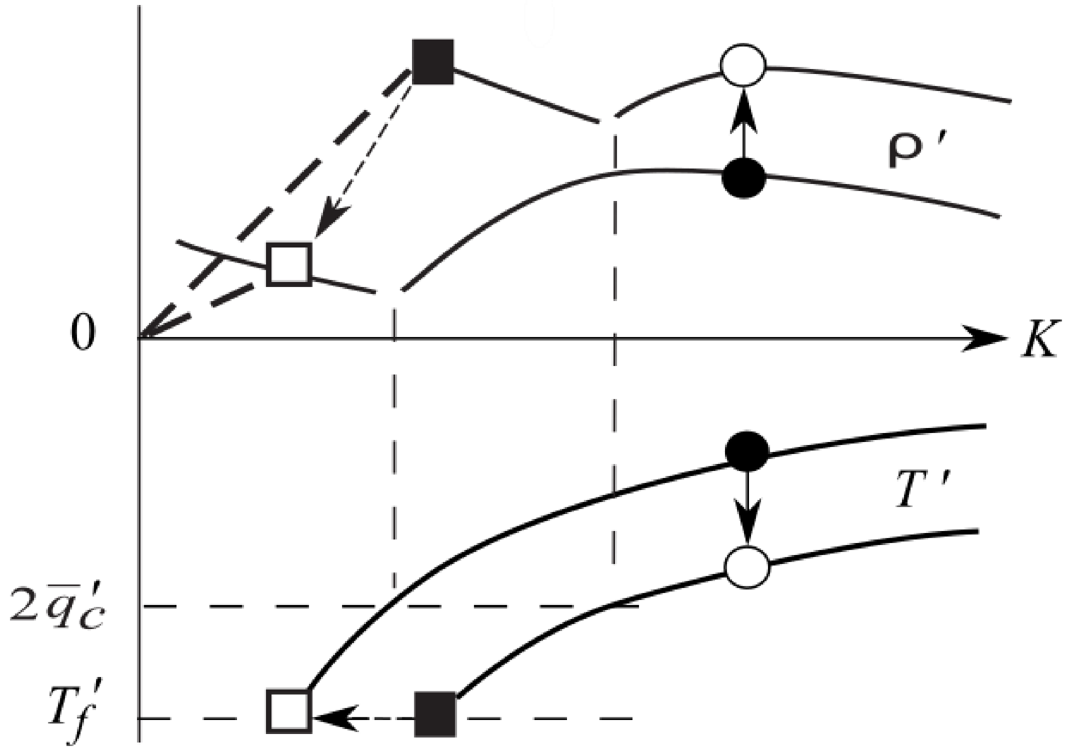

Figure 3: The evolution of the warm MEP when *q'* increases (solid arrows from solid to open circles) and the cold MEP when *q'* decreases (dashed arrows from solid to open squares). The thick dashed lines are the admittance lines associated with the cold MEP

https://doi.org/10.5194/cp-2021-94
Preprint. Discussion started: 20 July 2021

Climate of the Past Discussions

953 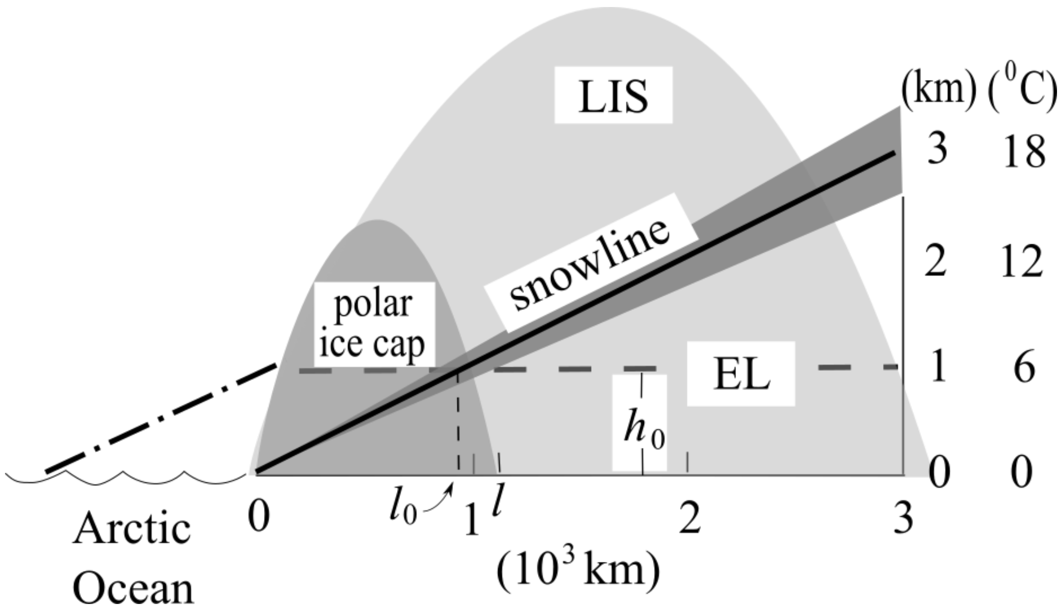

954 **Figure 4:** The summer SAT and snowline (aligned in the solid line) over the subpolar region
955 during the interglacial, the dark cone indicates their perturbation by the orbital forcing. The
956 ELA (h_0, dashed line) specifies the margin of the polar ice cap (medium shade). The dash-dot-
957 ted line marks the snowline when the polar ice cap may transition to the ice-free state with
958 strong warming. During the glacial, the summer SAT is at the freezing point (hence aligned
959 with the abscissa) and the ice sheet extends to the subtropical front (light shade)

960

https://doi.org/10.5194/cp-2021-94
Preprint. Discussion started: 20 July 2021

Climate of the Past
Discussions

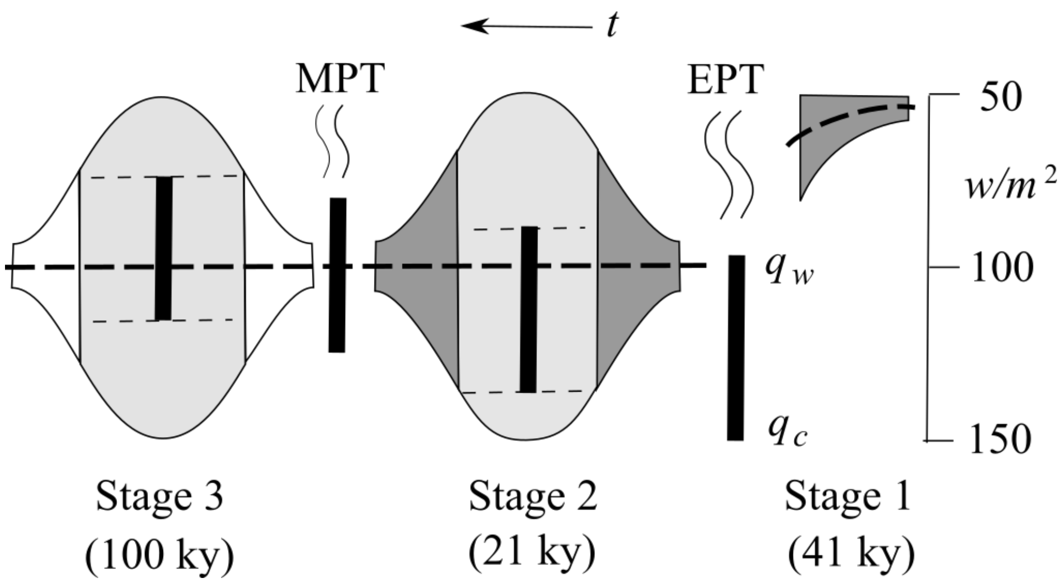

Figure 5: The evolution of the forcing envelop and ice signals during Pleistocene cooling, which consists of three stages and their transitions. The vertical bars are bistable intervals spanned by the cold (q_c) and warm (q_w) thresholds, which rise due to the Pleistocene cooling. Stage 1 is dominated by the interglacial cycles (hence dark-shaded) at the 41-ky obliquity period. Stage 2 sees the emergence of the G/IG cycles (hence light-shaded) at the 21-ky precession period. Stage 3 is dominated by the ice-age cycles (hence unshaded) at the 100-ky eccentricity period

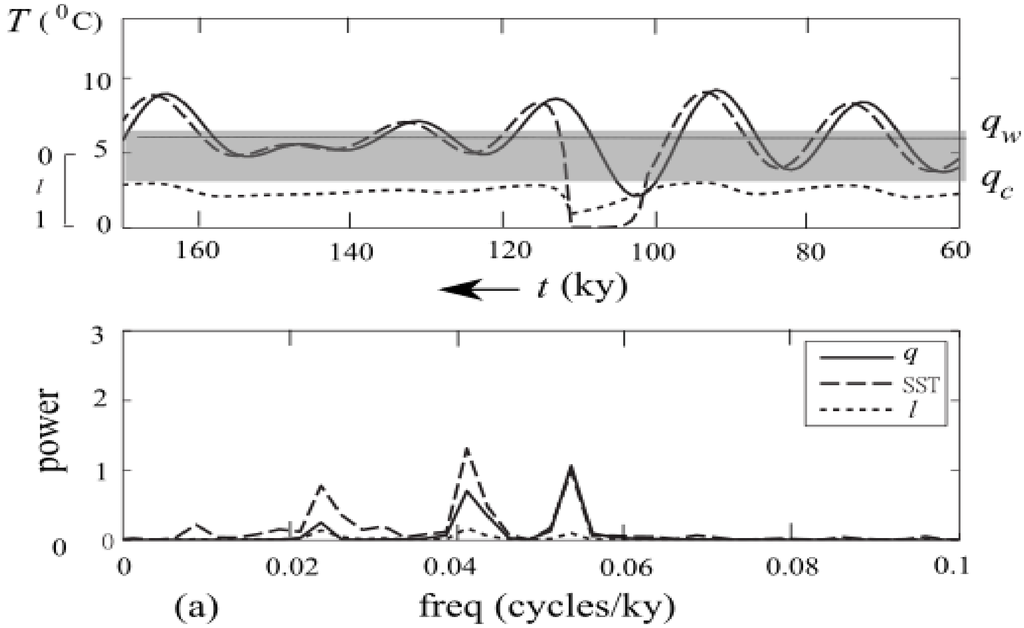

Figure 6(a): Timeseries and power spectra of the forcing (q, solid lines in equivalent temperature), subpolar SST (dashed, with a global-mean of 14 ^{0}C) and ice margin (l, dotted, in fractional extension into the subpolar). The thin horizonal line is the time-mean forcing and the bistate interval (shaded bar) is that of Stage 2 shown in Fig. 5, which allows the generation of the glacial state during high eccentricity, but the SST and ice-margin spectra remain dominated by the precession

https://doi.org/10.5194/cp-2021-94
Preprint. Discussion started: 20 July 2021

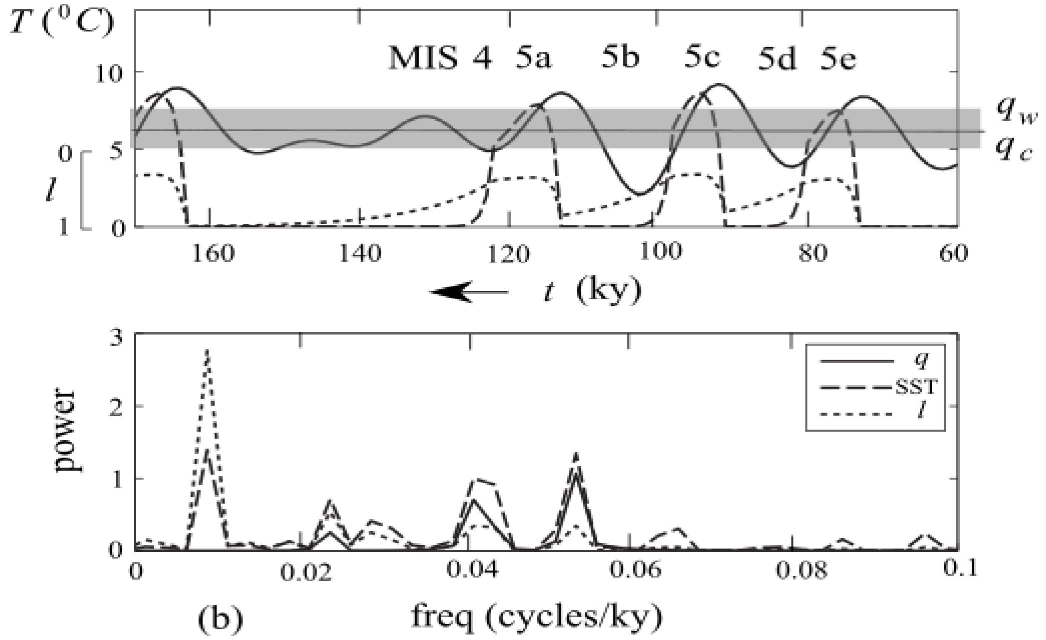

Figure 6(b): Same as Fig. 6a but for Stage 3 when the bistate interval (shaded bar) is further raised by Pleistocene cooling. There are both glacial and interglacial states during high eccentricity corresponding to the labelled marine isotope stages, but only the glacial state spanning the low eccentricity, allowing the full growth of the ice sheet. The SST and ice-margin spectra exhibit a strong peak at the eccentricity period despite its absence in the forcing spectrum